Advances in Computational Mathematics (2022) 48:58
https://doi.org/10.1007/s10444-022-09975-x

Polycircular domains, numerical conformal mappings, and moduli of quadrilaterals

Mohamed Nasser[1,2] · Oona Rainio[3] · Antti Rasila[4] · Matti Vuorinen[3] · Terry Wallace[4] · Hang Yu[5] · Xiaohui Zhang[5]

Received: 17 February 2022 / Accepted: 10 August 2022 / Published online: 13 September 2022

Abstract

We study numerical conformal mappings of planar Jordan domains with boundaries consisting of finitely many circular arcs, also called polycircular domains, and compute the moduli of quadrilaterals for these domains. Experimental error estimates are provided and, when possible, comparison to exact values or other methods are given. We also analyze the rate of convergence as a function of the number of degrees of freedom. The main ingredients of the computation are boundary integral equations combined with the fast multipole method.

Keywords Boundary integral equations · Condenser capacity · Numerical conformal mappings

Communicated by : Tobin Driscoll

✉ Oona Rainio
ormrai@utu.fi

Mohamed Nasser
mms.nasser@wichita.edu

Antti Rasila
antti.rasila@iki.fi; antti.rasila@gtiit.edu.cn

Matti Vuorinen
vuorinen@utu.fi

Hang Yu
yuhang_zstu@163.com

Xiaohui Zhang
xiaohui.zhang@zstu.edu.cn

[1] Department of Mathematics, Statistics, and Physics, Wichita State University, Wichita, KS 67260-0033, USA

[2] Department of Mathematics, Statistics and Physics, Qatar University, Doha, Qatar

[3] Department of Mathematics and Statistics, University of Turku, FI-20014 Turku, Finland

[4] Guangdong Technion, Shantou, Guangdong 515063, China

[5] School of Science, Zhejiang Sci-Tech University, Hangzhou 310018, China

Mathematics Subject Classification (2010) Primary 65E05 · Secondary 30C85 · 31A15

1 Introduction

Conformal mappings are essential for many applications of complex analysis. Examples include modeling of airfoils, analysis of turbulence, design of dams, and mathematical theory of electricity [1]. A first example is a mathematical model of a physical condenser, which is a domain $G \subset \mathbb{R}^2$ together with a compact set $E \subset G$ [41]. The pair (G, E) is called a *condenser* and its *capacity* is defined as [13]

$$\operatorname{cap}(G, E) = \inf_{u \in A} \int_G |\nabla u|^2 dm, \tag{1.1}$$

where A is the family of all harmonic functions with $u(x) \geq 1$ for all $x \in E$ and $u(x) \to 0$ when $x \to \partial G$, and dm is the 2-dimensional Lebesgue measure.

In real-world applications, the sets E and ∂G have a simple geometry. In other words, they both have a finite number of components and each component is a piecewise smooth curve. In this case, it is known that the infimum in (1.1) is attained by a harmonic function.

A second example is to solve the following Dirichlet-Neumann boundary value problem for the Laplace equation in a planar Jordan domain G with a piecewise smooth boundary $\partial G = \cup_{k=1}^{4} \partial G_k$ where the sets ∂G_k are piecewise smooth arcs and occur in positive order—the sets ∂G_k and the domain G define a *quadrilateral*. This problem can be formulated as

$$\begin{cases} \Delta u = 0, & \text{on } G, \\ u = 1, & \text{on } \partial G_1, \\ u = 0, & \text{on } \partial G_3, \\ \partial u/\partial \mathbf{n} = 0, & \text{on } \partial G_2, \\ \partial u/\partial \mathbf{n} = 0, & \text{on } \partial G_4, \end{cases}$$

where $\partial u/\partial \mathbf{n}$ denotes the directional derivative of u along the outward normal. If u is a solution function to this problem, then the expression $\int_G |\nabla u|^2 dm$ defines the *modulus* of the quadrilateral.

Sometimes, conformal mappings can be applied to simplify the geometry and, in fact, to solve this Dirichlet-Neumann problem. By the Riemann mapping theorem we know that a Jordan domain G is conformally equivalent to the unit disk, but this theorem does not give a clue for finding the conformal map. In the case of polygonal domains, widely used numerical methods based on the Schwarz-Christoffel transformation have been developed by D. Gaier [14], L.N. Trefethen and T.A. Driscoll [12], and N. Papamichael and N. Stylianopoulos [39]. Jordan domains bounded by finitely many circular arcs have been studied by P. Brown and M. Porter [8, 43], by U. Bauer and W. Lauf [4], and, in particular, by D. Crowdy [10]. D. Crowdy introduced the term *polycircular* to describe domains with boundaries consisting of finitely many circular

arcs or rectilinear segments and we will also use this term. See also [5, 22, 44]. Note that, if the Dirichlet-Neumann problem can be solved, then the conformal mapping can be recovered with the conjugate function method studied in [17].

We give here new numerical methods for this same case and present our results in the form of numerical tables, graphics, and analysis of algorithm performance. The method is based on boundary integral equations (R. Kress, [25]) as developed and implemented in a series of papers during the past two decades, see e.g. [28, 31]. The method uses the fast multipole method implementation from [16] for the speed-up of solving linear equations. In a recent series of papers [31, 34], the method was applied for the capacity computation of planar condensers and for the study of isoperimetric problems for capacity. In particular, we will make use of the very recent results in [31].

In this paper, we study the scope of applicability of this method to new kinds of problems, previously not studied by means of other methods. In particular, we study numerical conformal mapping of simply connected domains bounded by circular arcs and compute the values of an important domain functional, so-called *modulus of quadrilateral* for several such domains. One example is the standard letter *L*-shaped domain, studied in numerous papers but here the sides are not rectilinear segments but circular arcs. We also study a conjecture posed by Brown and Porter in [9], and solve it affirmatively. In a subsequent series of studies, we plan to apply the same method for the study of the way in which the condenser capacity $\mathrm{cap}(G, E)$ depends on the geometry of the sets E and G including isocapacitary problems.

The structure of this paper is as follows. In Section 2, we give the basic facts about the boundary integral method and its efficient implementation. Section 3 describes the method of Kress [23] for the treatment of non-smooth boundary points in numerical integration and a refinement principle in the trapezoid rule. Section 4 contains applications of the presented method to several polycircular quadrilaterals. Several numerical examples for the computation of the exterior modulus of quadrilaterals are presented in Section 5. Finally, in Section 6, the proposed method is applied to gear domains.

2 Preliminary notions

The capacity of a condenser defined in the introduction can be defined in many equivalent ways as shown in [13, 15]. First, the family A in (1.1) may be replaced by several other families of functions by [15, Lemma 5.21, p. 161]. Furthermore,

$$\mathrm{cap}\,(G, E) = \mathsf{M}(\Delta(E, \partial G; G)), \tag{2.1}$$

where $\Delta(E, \partial G; G)$ is the family of all curves joining E with the boundary ∂G in the domain G and M stands for the modulus of a curve family [13, 15, 20]. We often use the unit disk $\mathbb{B}^2 = \{x \in \mathbb{R}^2 : |x| < 1\}$ in the place of the domain G.

2.1 Quadrilaterals

A Jordan domain in the complex plane $\mathbb{C}$ is a domain with boundary homeomorphic to the unit circle. A *quadrilateral* is a Jordan domain D together with four

distinct points $z_1, z_2, z_3, z_4 \in \partial D$ which define a positive orientation of the boundary. In other words, if we traverse the boundary, then the points occur in the order of indices and the domain D is on the left hand side. The quadrilateral is denoted by $(D;z_1, z_2, z_3, z_4)$. The *modulus of the quadrilateral* is a unique positive number h such that D can be conformally mapped by some conformal map f onto the rectangle with vertices $0, 1, 1 + ih, ih$ such that [39, p. 52]

$$f(z_1) = 0, \quad f(z_2) = 1, \quad f(z_3) = 1 + ih, \quad f(z_4) = ih\,.$$

The modulus is denoted by $\operatorname{mod}(D;z_1, z_2, z_3, z_4)$. The following basic formula is often used:

$$\operatorname{mod}(D;z_1, z_2, z_3, z_4)\operatorname{mod}(D;z_2, z_3, z_4, z_1) = 1\,. \tag{2.2}$$

A simple example of a quadrilateral is the case when the domain D is a rectangle with sides a and b and the points z_1, z_2, z_3, z_4 are its vertices. Depending on the labeling of the vertices, the modulus is either a/b or b/a. An alternative equivalent definition is based on the Dirichlet-Neumann problem mentioned in the introduction [2, Thm 4.5, p. 63].

2.2 Quadrilateral modulus and curve families

The modulus of a quadrilateral $(D;z_1, z_2, z_3, z_4)$ is connected with the modulus of the family of all curves in D, joining the opposite boundary arcs (z_2, z_3) and (z_4, z_1), as follows

$$\operatorname{mod}(D;z_1, z_2, z_3, z_4) = \mathsf{M}(\Delta((z_2, z_3), (z_4, z_1);D))\,. \tag{2.3}$$

2.3 Grötzsch ring and elliptic integrals

A *ring domain*, or briefly a *ring*, in the plane is a domain whose complement has exactly two components. Such a domain can be conformally mapped onto $\{z \in \mathbb{C} : r < |z| < 1\}$. The number $\log(1/r)$ is called *the modulus of the ring*. One can also consider a ring R with complementary components $E, F \subset \mathbb{C}$ as a condenser $(\mathbb{C} \setminus E, F)$ and define the capacity of the ring as

$$\operatorname{cap} R = \operatorname{cap}(\mathbb{C} \setminus E, F) = 2\pi/\operatorname{mod} R.$$

The formula (2.1) gives now the connection between the modulus of a ring and the modulus of the family of curves joining its boundary components. The so-called Grötzsch ring $G_r = \mathbb{B}^2 \setminus [0, r]$, $0 < r < 1$, is frequent in the study of capacities. The following explicit formulas hold for the capacity of this ring [20, (7.18), p. 122],

$$\operatorname{cap} G_r = \frac{2\pi}{\mu(r)}\,; \quad \mu(r) = \frac{\pi}{2}\frac{\mathcal{K}'(r)}{\mathcal{K}(r)}, \tag{2.4}$$

where $\mathcal{K}(r)$ and $\mathcal{K}'(r)$ are the elliptic integrals of the first kind

$$\mathcal{K}(r) = \int_0^1 \frac{dx}{\sqrt{(1-x^2)(1-r^2x^2)}}, \quad \mathcal{K}'(r) = \mathcal{K}(r'), \quad r' = \sqrt{1-r^2}\,. \tag{2.5}$$

The elliptic integrals $\mathcal{E}(r)$ and $\mathcal{E}'(r)$ of the second kind are

$$\mathcal{E}(r) = \int_0^{\pi/2} \sqrt{1 - r^2 \sin^2 x}\, dx, \quad \mathcal{E}'(r) = \mathcal{E}(r'). \tag{2.6}$$

The above function μ is recurrent in the study of conformal invariants and also in our work below.

2.4 History of numerical conformal mapping

The historical account of function theory [6] also describes the origin and evolution of the Schwarz-Christoffel formula. During the past fifty years, the development of computational methods has made it possible to use this formula and other methods of function theory for many applications and to develop the general theory of numerical conformal mappings, see [12, 14, 26, 38, 39, 42, 45]. A short overview of the literature is given in [39, pp. 14–16] and [26, pp. 8–12]. For a comprehensive survey, see [45].

3 Boundary integral method

3.1 The integral equation

We assume that the boundary $\Gamma = \partial G$ is a smooth Jordan curve parametrized by a 2π-periodic function $\eta : [0, 2\pi] \to \Gamma$ which is twice continuously differentiable and satisfies $\eta'(t) \neq 0$ for all $t \in [0, 2\pi]$ (piecewise smooth boundaries will be considered in the next subsection). The boundary Γ is oriented such that G is to the left of Γ, i.e., Γ is oriented counterclockwise for bounded G and clockwise for unbounded G. We denote by H the space of all Hölder continuous real-valued functions on the boundary Γ.

Let $A : [0, 2\pi] \to \mathbb{C} \setminus \{0\}$ be the complex function

$$A(t) = \begin{cases} \eta(t) - \alpha, & \text{if } G \text{ is bounded}, \\ 1, & \text{if } G \text{ is unbounded}, \end{cases} \tag{3.1}$$

where α is a given auxiliary point in the domain G. The generalized Neumann kernel $N(s, t)$ is defined by [46]

$$N(s,t) := \frac{1}{\pi} \operatorname{Im}\left(\frac{A(s)}{A(t)} \frac{\eta'(t)}{\eta(t) - \eta(s)}\right), \quad t \neq s, \tag{3.2}$$

$$N(t,t) := \frac{1}{\pi}\left(\frac{1}{2} \operatorname{Im} \frac{\eta''(t)}{\eta'(t)} - \operatorname{Im} \frac{A'(t)}{A(t)}\right). \tag{3.3}$$

The kernel $N(s,t)$ is continuous on $[0,2\pi]\times[0,2\pi]$ and hence, the integral operator $\mathbf{N}$ defined on H by

$$\mathbf{N}\gamma(s) := \int_0^{2\pi} N(s,t)\gamma(t)\,dt, \quad s\in[0,2\pi],$$

is compact. The integral equation involves also the kernel

$$M(s,t) := \frac{1}{\pi}\,\mathrm{Re}\left(\frac{A(s)}{A(t)}\,\frac{\eta'(t)}{\eta(t)-\eta(s)}\right), \quad s\neq t, \tag{3.4}$$

which is singular and has the representation

$$M(s,t) = -\frac{1}{2\pi}\cot\frac{s-t}{2} + M_1(s,t). \tag{3.5}$$

Here the kernel M_1 is continuous on $[0,2\pi]\times[0,2\pi]$ where

$$M_1(t,t) := \frac{1}{\pi}\left(\frac{1}{2}\,\mathrm{Re}\,\frac{\eta''(t)}{\eta'(t)} - \mathrm{Re}\,\frac{A'(t)}{A(t)}\right). \tag{3.6}$$

The integral operator $\mathbf{M}$ defined on H by

$$\mathbf{M}\gamma(s) := \int_0^{2\pi} M(s,t)\gamma(t)dt, \quad s\in[0,2\pi],$$

is singular, but is bounded on H [46].

Theorem 3.1 *For a given function $\gamma\in H$, there exists a unique function $\rho\in H$ and a unique constant h such that the formula*

$$\frac{\gamma+h+\mathrm{i}\rho}{A} \tag{3.7}$$

defines the boundary values of an analytic function f in G with $f(\infty)=0$ for unbounded G. The function ρ is the unique solution of the integral equation

$$(\mathbf{I}-\mathbf{N})\rho = -\mathbf{M}\gamma \tag{3.8}$$

and the constant h is given by

$$h = (\mathbf{M}\rho - (\mathbf{I}-\mathbf{N})\gamma)/2. \tag{3.9}$$

A MATLAB function `fbie` for solving the integral equation (3.8) is presented in [29]. In this function `fbie`, the integral equation (3.8) is discretized by the Nyström method with the trapezoidal rule to obtain an $n\times n$ linear system $(I-B)\mathbf{x}=\mathbf{y}$, where n is the number of nodes in the discretization of the boundary Γ and B is the discretization matrix of the operator $\mathbf{N}$. Computing the right-hand side of the linear system involves the computation of the FFT which can be computed in $O(n\log n)$ operations (see [29, p. 200]). For solving thelinear system $(I-B)\mathbf{x}=\mathbf{y}$, the GMRES method is

applied where the matrix-vector product in the GMRES method is computed by means of the MATLAB function `zfmm2dpart` in the toolbox `FMMLIB2D` [16]. Each iteration of GMRES requires $O(n)$ operations. The number of GMRES iterations required to obtain a very good approximation to the exact solution is mostly independent of n. Further, only a few steps of GMRES are enough to reduce the relative residual norm to 0.5×10^{-14} or smaller. See e.g., [29]. Thus, computational cost of the presented method is $O(n \log n)$ operations.

Let `et`, `etp`, `A`, `gam`, and `rho`, be $n \times 1$ discretization vectors of the functions $\eta(t)$, $\eta'(t)$, $A(t)$, $\gamma(t)$, and $\rho(t)$, respectively. Then, the $n \times 1$ vectors `rho` and `h` are computed by

$$[\texttt{rho}, \texttt{h}] = \texttt{fbie}(\texttt{et}, \texttt{etp}, \texttt{A}, \texttt{gam}, \texttt{n}, \texttt{iprec}, \texttt{restart}, \texttt{gmrestol}, \texttt{maxit}).$$

Theoretically, all elements of the vector `h` are equal to a constant h in (3.9). Numerically, we will approximate the constant h by the arithmetic mean of the elements of the vector `h`. For the other parameters in `fbie`, we choose `iprec`=5, `gmrestol`= 0.5×10^{-14}, `restart` = [ ], and `maxit`=100. This means that the tolerances of the methods are 0.5×10^{-15} for FMM and 0.5×10^{-14} for GMRES. Moreover, the GMRES is used without restart, and the maximum number of GMRES iterations is 100. The auxiliary points α in (3.1) need to be chosen sufficiently far away from the boundary Γ. For some domains (see Examples 4.10 and 4.12 below), we need to choose α carefully to ensure the convergence of the method.

3.2 Kress method

In this paper, we shall assume that Γ is a piecewise smooth Jordan curve with a finite number of corner points such that none of these corner points is a cusp. We assume that the tangent vector of the boundary has only the first kind discontinuity at each corner point where the left tangent vector at each corner point is considered as the tangent vector at this point. For such boundaries Γ, the integral operator with the generalized Neumann kernel (3.8) is not compact, but this operator can be written as a sum of a compact operator and bounded non-compact operator with norm less than one in suitable function spaces [32]. Hence, we can apply the Fredholm theory to the integral equation with the generalized Neumann kernel although the operator is not compact [23].

Using the method described above to solve the integral equation (3.8) when Γ is a piecewise smooth Jordan curve yields only poor convergence since the solution of the integral equation (3.8) has a singularity in its first derivative in the vicinity of the corner points [23, 32]. To achieve a satisfactory accuracy, we first remove the discontinuity of the derivatives of the solution of the integral equation at the corner points by using a suitable substitution [23, 24]. Then, the transformed equation can be solved using the above method.

Following Kress [23, 24], we define a bijective function $w : [0, 2\pi] \to [0, 2\pi]$ by

$$w(t) = 2\pi \frac{[v(t)]^p}{[v(t)]^p + [v(2\pi - t)]^p}, \tag{3.10}$$

where

$$v(t) = \left(\frac{1}{p} - \frac{1}{2}\right)\left(\frac{\pi - t}{\pi}\right)^3 + \frac{1}{p}\frac{t-\pi}{\pi} + \frac{1}{2}.$$

The function w is strictly monotonically increasing and infinitely differentiable function, and the integer $p \geq 2$ is the grading parameter.

Assume that the boundary Γ has $m > 0$ corner points and is parametrized by a 2π-periodic function $\hat{\eta}(t)$ such that

$$\hat{\eta}(0), \quad \hat{\eta}(2\pi/m), \quad \hat{\eta}(4\pi/m), \quad \ldots, \quad \hat{\eta}(2(m-1)\pi/m) \tag{3.11}$$

are the corner points of Γ. Assume also that $\hat{\eta}(t)$ is twice continuously differentiable with $\hat{\eta}'(t) \neq 0$ for all $t \in [0, 2\pi]\backslash\{0, 2\pi/m, \ldots, 2(m-1)\pi/m\}$. Then we define a bijective, strictly monotonically increasing and infinitely differentiable function, $\delta : [0, 2\pi] \to [0, 2\pi]$, by [27]

$$\delta(t) = \begin{cases} w(mt)/m, & t \in [0, 2\pi/m), \\ [w(mt - 2\,pi) + 2\pi]/m, & t \in [2\pi/m, 4\pi/m), \\ \quad \vdots & \\ [w(mt - 2(m-1)\pi) + 2(m-1)\pi]/m, & t \in [2(m-1)\pi/m, 2\pi]. \end{cases}$$

The function δ is at least p times continuously differentiable since the function w has a zero of order p at the endpoints $t = 0$ and $t = 2\pi$ [23, Theorem 2.1].

Then, we parametrize the boundary Γ by $\eta(t) = \hat{\eta}(\delta(t))$ and hence $\eta'(t) = \hat{\eta}'(\delta(t))\delta'(t)$, $t \in [0, 2\pi]$. With the new parametrization, the integral equation (3.8) is solved accurately using the above-mentioned function `fbie` as in the case of domains with smooth boundaries.

By [23, Theorems 2.1 and 4.4], the error in the computed approximate values is less than $Cn^{-(2q+1)}$ where q is an integer such that $2q + 1 \leq \hat{\alpha}p$ where $0 < \hat{\alpha} < 1$ and the constant C depends on $\hat{\alpha}$, q, and the integrand. The constant $\hat{\alpha}$ depends on the integrand which in turns depends on the parametrization $\eta(t)$ (see [23, Section 2] for more details). It seems from the inequality$2q + 1 \leq \hat{\alpha}p$ that choosing large values of p increases the order of convergence of the method. However, large values of p in (3.10) cause the discretization points to be accumulated around the corner points, because of which some of these discretization points might be nearly equal for large values of n in double precision floating point calculations. So, in our numerical experiments below, we choose $p = 4$. The numerical results presented below in Figs. 3 and 13 illustrate that the order of the convergence of the presented method is $O(n^{-4})$ for the examples presented in Sections 4.1 and 5.1.

3.3 Parametrizing the boundaries of polygonal domains

In this paper, we assume that the boundary Γ is a polygon consisting of a finite number of finite segments, circular arcs, or both segments and circular arcs. The

boundary Γ will be parametrized as described in the preceding subsection. We discretize the interval $[0, 2\pi]$ by n equidistant nodes,

$$t_k = (k-1)\frac{2\pi}{n}, \quad k = 1, \ldots, n. \tag{3.12}$$

Then the parametrization of the boundary Γ is discretized by $\eta(s_1), \eta(s_s), \ldots, \eta(s_n)$ where $s_k = \delta(t_k)$, $k = 1, 2, \ldots, n$. Similarly, the derivative of the parametrization of the boundary is discretized by $\eta'(s_k)s'_k$ where $s'_k = \delta'(t_k)$, $k = 1, 2, \ldots, n$. A MATLAB function `plgsegcirarcp.m` for computing such a parametrization can be downloaded from https://github.com/mmsnasser/circa. To use this MATLAB function, assume that Γ is a polygon with m finite vertices $v_1, v_2, \ldots, v_m$ with $v_{m+1} = v_1$. For the parametrization $\eta(t)$ of the boundary Γ, it follows from (3.11) and (3.12) that

$$v_k = \eta\Big((k-1)\frac{2\pi}{m}\Big) = \eta\big(t_{(k-1)n/m+1}\big), \quad k = 1, 2, \ldots, m. \tag{3.13}$$

For $k = 1, 2, \ldots, m$, we assume that the center of the portion of the boundary between v_k and v_{k+1} is c_k if the portion is a circular arc and $c_k = \infty$ if the portion is a segment. Further, if the portion of the boundary between v_k and v_{k+1} is a circular arc, then we introduce an indicator d_k for it with value 1 if the arc is positively oriented with respect to the pertaining circle center c_k and -1 otherwise. For segment portions of the boundary this indicator is $d_k = 0$. We assume here that n is an integer multiple of m so that each side of the polygon will be discretized by n/m points. Define the vectors

$$\mathtt{v} = [\mathtt{v}_1, \ldots, \mathtt{v}_n], \quad \mathtt{c} = [\mathtt{c}_1, \ldots, \mathtt{c}_n], \quad \mathtt{d} = [\mathtt{d}_1, \ldots, \mathtt{d}_n],$$

Then, discretizations of the parametrization of the boundary and its derivative can be computed using the MATLAB function `plgsegcirarcp.m` by calling

$$[\mathtt{et}, \mathtt{etp}] = \mathtt{plgsegcirarcp}(\mathtt{v}, \mathtt{c}, \mathtt{d}, \mathtt{n}/\mathtt{m}).$$

3.4 Conformal mapping onto the unit disk

In this subsection, we review a numerical method for the computation of the conformal mapping $w = \Phi(z)$ from a polygonal domain G onto the unit disk $\mathbb{B}^2 = \Phi(G)$ [30, 35].

For a bounded domain G, let $\gamma = -\log|\eta(t) - \alpha|$, let ρ be the unique solution of the integral equation (3.8), and let the constant h be given by (3.9). Then, the mapping function Φ with the normalization

$$\Phi(\alpha) = 0, \quad \Phi'(\alpha) > 0 \tag{3.14}$$

can be written for $z \in G \cup \Gamma$ as

$$\Phi(z) = c(z-\alpha)e^{(z-\alpha)f(z)} \tag{3.15}$$

where $c = \Phi'(\alpha) > 0$ and the function $f(z)$ is analytic in G with the boundary values $A(t)f(\eta(t)) = \gamma(t) + h + \mathrm{i}\rho(t)$. The boundary values of the conformal mapping are now given by

$$\Phi(\eta(t)) = c(\eta(t) - \alpha)e^{\gamma(t)+h+\mathrm{i}\rho(t)}.$$

Since $|\Phi(\eta(t))| = 1$, it follows that $\Phi(\eta(t))$ can be written as

$$\Phi(\eta(t)) = e^{\mathrm{i}S(t)}, \quad t \in [0, 2\pi], \tag{3.16}$$

where

$$S(t) = \arg(\eta(t) - \alpha) + \rho(t) \tag{3.17}$$

is a one-to-one increasing function on $[0, 2\pi]$ with $S(2\pi) - S(0) = 2\pi$. The function $S(t)$ is known as the boundary correspondence function [21, p. 380]. Differentiation yields

$$S'(t) = \operatorname{Im}\left[\frac{\eta'(t)}{\eta(t) - \alpha}\right] + \rho'(t).$$

When G is an unbounded domain, we assume $\gamma = \log|\eta(t) - z_1|$ where z_1 is a given point in the exterior domain of G, i.e., z_1 is in the bounded domain enclosed by Γ. We assume also that ρ is the unique solution of the integral equation (3.8) and the constant h is given by (3.9). Then, the mapping function Φ with the normalization

$$\Phi(\infty) = 0, \quad \lim_{z\to\infty}(z\Phi(z)) > 0$$

can be written for $z \in G \cup \Gamma$ as

$$\Phi(z) = \frac{c}{z - z_1}e^{f(z)} \tag{3.18}$$

where $c = \lim_{z\to\infty}(z\Phi(z)) > 0$ and the function $f(z)$ is analytic in G with the boundary values $A(t)f(\eta(t)) = \gamma(t) + h + \mathrm{i}\rho(t)$ and $f(\infty) = 0$. Note that $A(t) = 1$ for unbounded domains. Hence, the boundary values of the conformal mapping are given by

$$\Phi(\eta(t)) = \frac{c}{\eta(t) - z_1}e^{\gamma(t)+h+\mathrm{i}\rho(t)}.$$

The mapping function Φ maps the boundary Γ onto the unit circle $\partial\mathbb{B}^2 = \Phi(\Gamma)$. Although the orientation of Γ is clockwise (G is on the left of Γ), the orientation of $\partial\mathbb{B}^2$ will be counterclockwise. Then $|\Phi(\eta(t))| = 1$ and hence $\Phi(\eta(t))$ can be written as in (3.16) where

$$S(t) = -\arg(\eta(t) - z_1) + \rho(t) \tag{3.19}$$

is a one-to-one increasing function on $[0, 2\pi]$ with $S(2\pi) - S(0) = 2\pi$. By differentiation, we obtain

$$S'(t) = -\operatorname{Im}\left[\frac{\eta'(t)}{\eta(t) - z_1}\right] + \rho'(t).$$

For both bounded and unbounded G, the function $\rho(t)$ is computed by solving the integral equation (3.8) and its derivative $\rho'(t)$ is computed by approximating $\rho(t)$ by a trigonometric interpolating polynomial and then differentiating the interpolating polynomial. This polynomial can be computed with FFT [45]. Then the boundary correspondence function $S(t)$ is computed through (3.17) for bounded G and by (3.19) for unbounded G. The boundary values of the mapping function Φ can be computed through (3.16). Thus, the function

$$\zeta(t) = \Phi(\eta(t)) = e^{\mathrm{i}S(t)}, \quad t \in [0, 2\pi], \tag{3.20}$$

is a parametrization of the unit circle. The values of the mapping function $w = \Phi(z)$ for $z \in D$ as well as the values of the inverse mapping function $z = \Phi^{-1}(w)$ for $w \in \mathbb{B}^2$ can be computed using the Cauchy integral formula. For the direct mapping, we have

$$\Phi(z) = \frac{1}{2\pi\mathrm{i}} \int_\Gamma \frac{\Phi(\eta)}{\eta - z} d\eta = \frac{1}{2\pi\mathrm{i}} \int_0^{2\pi} \frac{\Phi(\eta(t))}{\eta(t) - z} \eta'(t) dt = \frac{1}{2\pi\mathrm{i}} \int_0^{2\pi} \frac{\zeta(t)}{\eta(t) - z} \eta'(t) dt, \quad z \in D.$$

For the inverse mapping, we have

$$\Phi^{-1}(w) = \frac{1}{2\pi\mathrm{i}} \int_{\partial\mathbb{B}^2} \frac{\Phi^{-1}(\zeta)}{\zeta - w} d\zeta = \frac{1}{2\pi\mathrm{i}} \int_0^{2\pi} \frac{\Phi^{-1}(\zeta(t))}{\zeta(t) - w} \zeta'(t) dt = \frac{1}{2\pi\mathrm{i}} \int_0^{2\pi} \frac{\eta(t)}{\zeta(t) - w} \zeta'(t) dt, \quad w \in \mathbb{B}^2. \tag{3.21}$$

The mapping function Φ maps the vertices v_k, $k = 1, 2, \ldots, m$, of the polycircular domain D onto points $w_k = \Phi(v_k)$, $k = 1, 2, \ldots, m$, on the unit circle. In literature, the points $w_k, k = 1, 2, \ldots, m$ are known as the preimages of the vertices $v_k, k = 1, 2, \ldots, m$. In view of (3.13), it follows from (3.20) that the preimages are given by

$$w_k = \zeta(t_{(k-1)n/m+1}) = e^{\mathrm{i}S(t_{(k-1)n/m+1})}, \quad k = 1, 2, \ldots, m.$$

The implementation of the method presented in this subsection is given in the following MATLAB function `mapdisk.m`.

```
function [zet,zetp,c,S,Sp] = mapdisk(et,etp,n,zz,type)
if type=='b'
    A = et-zz; k = 1;
elseif type=='u'
    A = ones(size(et)); k = -1;
end
gam     = -k*log(abs(et-zz));
[rho,h] =  fbie(et,etp,A,gam,n,5,[],1e-14,200);
c       =  exp(-mean(h));
S       =  k*carg(et-zz)+rho;
Sp      =  k*imag(etp./(et-zz))+derfft(rho);
zet     =  exp(i*S);  zetp  =  exp(i*S).*i.*Sp;
end
```

All computer codes of the computations presented in this paper can be found in the link https://github.com/mmsnasser/circa.

3.5 Modulus of quadrilaterals

Consider the quadrilateral $(D;z_1,z_2,z_3,z_4)$ where D is a bounded simply connected polygonal domain and z_1,z_2,z_3,z_4 are four distinct points on ∂D with counterclockwise orientation. The modulus $\mathrm{mod}\,(D;z_1,z_2,z_3,z_4)$ can be computed in two steps. In the first step, we map the domain D using the conformal mapping $w=\Phi(z)$ described in Section 3.4 onto the unit disk $\mathbb{B}^2$ as shown in Fig. 1. The boundary ∂D is then mapped onto the unit circle. Here, the points z_1,z_2,z_3,z_4 need not be the vertices of the polygon. Assume that $z_k=\eta(\hat{t}_k)$ where $\hat{t}_k\in[0,2\pi]$, $k=1,2,3,4$. Then the four points z_1,z_2,z_3,z_4 will be mapped onto four points w_1,w_2,w_3,w_4 on the unit circle where, by (3.16), $w_k=e^{\mathrm{i}S(\hat{t}_k)}$, $k=1,2,3,4$. By the conformal invariance of the modulus, we have

$$\mathrm{mod}\,(D;z_1,z_2,z_3,z_4)=\mathrm{mod}\left(\mathbb{B}^2;w_1,w_2,w_3,w_4\right).$$

In the second step, the modulus $\mathrm{mod}\,(D;w_1,w_2,w_3,w_4)$ will be computed using the exact formula [39, (2.6.1)]

$$\mathrm{mod}\left(\mathbb{B}^2;w_1,w_2,w_3,w_4\right)=\frac{2}{\pi}\mu\left(1/\sqrt{k}\right),\quad k=|w_1,w_2,w_3,w_4|, \tag{3.22}$$

where the absolute (cross) ratio $|w_1,w_2,w_3,w_4|$ is defined by [20, p. 33]

$$|w_1,w_2,w_3,w_4|=\frac{|w_1-w_3||w_2-w_4|}{|w_1-w_2||w_2-w_4|}. \tag{3.23}$$

(Note that the definition of the cross-ratio here is different from the definition in [39, (1.10.5)].)

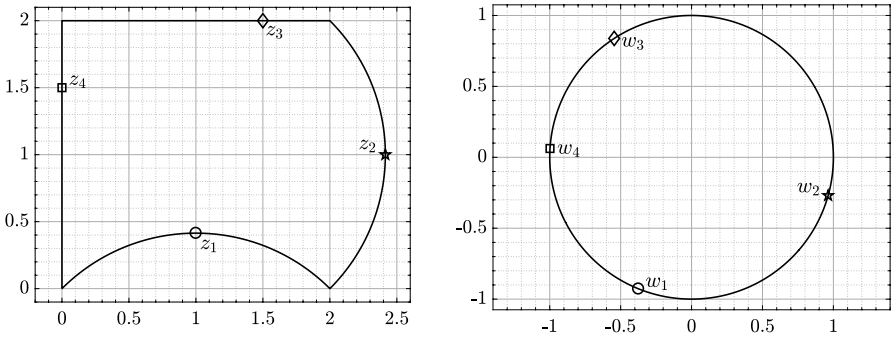

Fig. 1 The quadrilateral $(D;z_1,z_2,z_3,z_4)$ (left) and the quadrilateral $(\mathbb{B}^2;w_1,w_2,w_3,w_4)$ (right)

3.6 Exterior modulus of quadrilaterals

Let D be a bounded simply connected polygonal domain and let $D^- = \overline{\mathbb{C}}\backslash D$ be its complement with respect to the extended complex plane $\overline{\mathbb{C}} = \mathbb{C} \cup \{\infty\}$. We consider the quadrilateral $(D;z_1, z_2, z_3, z_4)$ where z_1, z_2, z_3, z_4 are four distinguished points on $\Gamma = \partial D$ with clockwise orientation. The exterior modulus of a quadrilateral $(D;z_1, z_2, z_3, z_4)$ equals the modulus of the family of all curves in D^- joining the opposite boundary arcs (z_2, z_3) and (z_4, z_1).

As in the bounded case, the unbounded domain D^- can be mapped using the conformal mapping $w = \Phi(z)$ described in Section 3.4 onto the unit disk $\mathbb{B}^2$ so that the four points z_1, z_2, z_3, z_4 on ∂D (in clockwise orientation) are mapped onto four points w_1, w_2, w_3, w_4 on the unit circle $\partial\mathbb{B}^2$ (in counterclockwise orientation). Assume that $z_k = \eta(\hat{t}_k)$ where $\hat{t}_k \in [0, 2\pi]$, then (3.16) implies that $w_k = e^{\mathrm{i}S(\hat{t}_k)}$, $k = 1, 2, 3, 4$. By the conformal invariance of the modulus, the exterior modulus of the quadrilateral $(D;z_1, z_2, z_3, z_4)$ is equal to $\mathrm{mod}\,(\mathbb{B}^2;w_1, w_2, w_3, w_4)$ which can be computed using the exact formula (3.22).

4 Examples: moduli of quadrilaterals

4.1 Half disk

Let

$$A = \{z \in \mathbb{C} : |z| < 1, \mathrm{Im} z > 0\}, \quad -1 < r < s < 1, 0 < \sigma < \beta < \pi.$$

Then $(A;z_1, z_2, z_3, z_4)$ where $z_1 = r$, $z_2 = s$, $z_3 = e^{\mathrm{i}\sigma}$, $z_4 = e^{\mathrm{i}\beta}$, is a quadrilateral, as can be seen from Fig. 2, and its modulus can be computed by means of elementary conformal mappings and it is

$$\mathrm{mod}\,(A;z_1, z_2, z_3, z_4) = \frac{\pi}{2} \frac{1}{\mu(1/\sqrt{u})}, \tag{4.1}$$

where

$$u = |f_1(\exp(\mathrm{i}\beta))^2, f_1(r)^2, f_1(s)^2, f_1(\exp(\mathrm{i}\sigma))^2|, \quad f_1(z) = \frac{1+z}{1-z}. \tag{4.2}$$

The approximate numerical values of the modulus $\mathrm{mod}\,(A;z_1, z_2, z_3, z_4)$ are computed by the above described method with $n = 2^{13}$ and the exact values are presented in Table 1. The relative error in the approximate values is also presented in Table 1 which is of order 10^{-14}. The relative error in the approximate values of the modulus of the half disk quadrilateral with $r = -0.5$, $s = 0.5$, $\sigma = \pi/4$, and $\beta = 3\pi/4$ obtained by the presented method for several values of n is presented in Fig. 3, which indicates clearly that the error is $O(n^{-4})$.

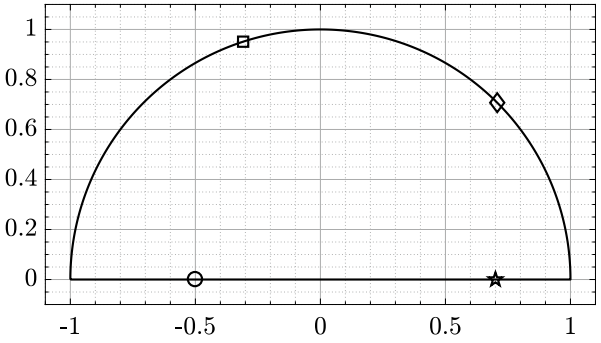

Fig. 2 Half disk quadrilateral with $z_1 = -0.5$, $z_2 = 0.7$, $z_3 = e^{\pi \mathrm{i}/4}$, and $z_4 = e^{3\pi \mathrm{i}/5}$

Table 1 The values of the modulus of the half disk quadrilateral obtained with $n = 2^{13}$ for several values of $r, s, \sigma = m\pi, \beta = \ell\pi$

r	s	m	ℓ	Exact Value	Approx. Value	Relative Error
−0.8	0.2	1/8	1/3	1.12275580085474	1.12275580085477	2.71×10^{-14}
−0.5	0.3	1/6	2/5	0.96809243696619	0.96809243696621	2.10×10^{-14}
−0.2	0.5	1/5	1/2	0.79872083257913	0.79872083257913	1.14×10^{-14}
0.2	0.6	1/4	3/5	0.95886428362598	0.95886428362597	1.83×10^{-14}
0.2	0.8	1/4	4/5	0.83635871682559	0.83635871682557	2.83×10^{-14}

4.2 Trapezoid

In this example, we consider the trapezoid T with the vertices $z_1 = 0$, $z_2 = 1$, $z_3 = 1 + \mathrm{i}L$, $z_4 = \mathrm{i}(L-1)$ (see Fig. 4 (left)). The exact value of the modulus $\mathrm{mod}\,(T; z_1, z_2, z_3, z_4)$ is given for $L > 1$ by [39, p. 82]

$$\mathrm{mod}\,(T; z_1, z_2, z_3, z_4) = \frac{\pi}{2\mu(k)}, \tag{4.3}$$

where

$$k = \frac{1 - 2\lambda\lambda'}{1 + 2\lambda\lambda'}, \quad \lambda = \mu^{-1}\left(\frac{\pi}{2(2L-1)}\right), \quad \lambda' = \sqrt{1 - \lambda^2}.$$

The above method with $n = 2^{13}$ is used to compute approximate values of the modulus $\mathrm{mod}\,(T; z_1, z_2, z_3, z_4)$ for several values of $L \in (1, 5]$. The relative error in the computed values is presented in Fig. 4. The values of the function μ and its inverse are computed as described in [36]. Figure 4 presents also the relative error in the approximate values obtained with the SC Toolbox [11]. As we see from the figures, for $L > 2.5$, the relative errors of the two methods are almost identical. For small L, the results obtained with SC Toolbox are better than the results obtained by the proposed method, which is expected since the Schwarz–Christoffel mapping is the standard method for computing the conformal mapping from polygonal simply

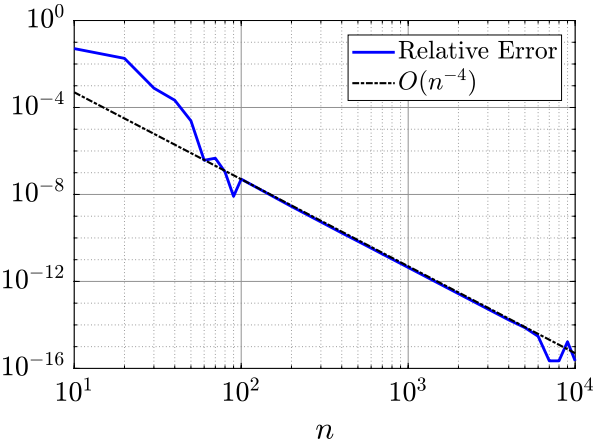

Fig. 3 The relative error in the approximate values of the modulus of the half disk quadrilateral vs. n

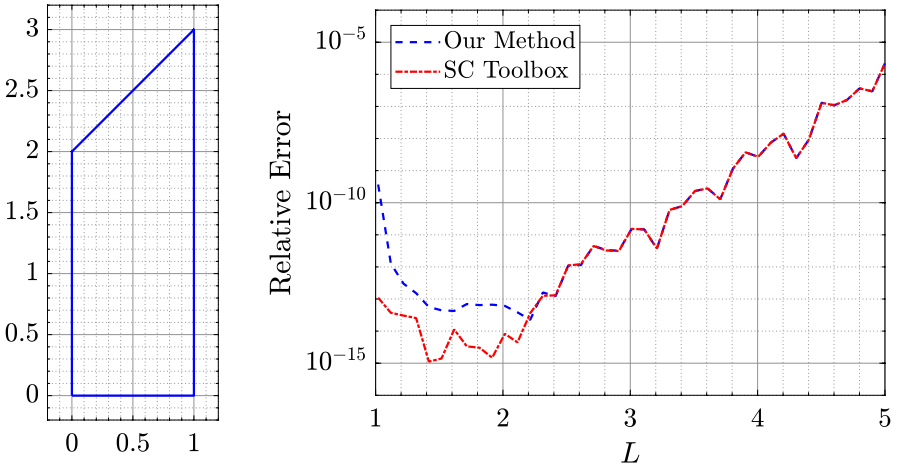

Fig. 4 The trapezoid T for $L = 3$ (left) and the relative error in the computed approximate values of the modulus vs L for the trapezoid (right)

connected domain onto the unit disk. Further, when L is very close to 1, the side $[z_4, z_1] = [\mathrm{i}(L-1), 0]$ becomes too small compared to the other sides of the trapezoid and hence the collocation points on this segments might be so close to each other that the error for the presented method is larger than the error for the SC Toolbox. Also for $1.4 \leq L \leq 2.2$, the error of the presented method is less than 10^{-13} in Fig. 4, which is accurate enough since we have chosen the accuracy of the GMRES to be 10^{-14} and the accuracy of the FMM method to be 0.5×10^{-14}. For $L > 2.5$, the domain becomes elongated and the error for both methods increases as L increases, possibly due to the effect of the crowding phenomenon.

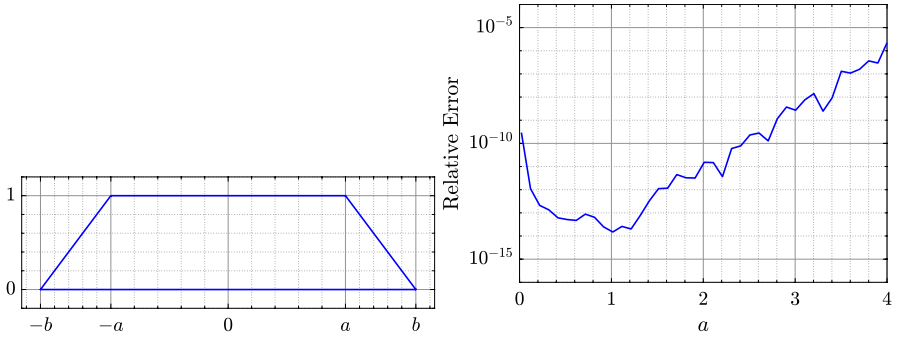

Fig. 5 The symmetric trapezoid P (left) and the relative error in the computed approximate values of the modulus vs a (right)

4.3 Symmetric trapezoid

Let $a, b > 0$ and consider the polygon P with the vertices $z_1 = -a + \mathrm{i}$, $z_2 = -b$, $z_3 = b$, and $z_4 = a + \mathrm{i}$. Then, by symmetry,

$$\mathrm{mod}\,(P; z_1, z_2, z_3, z_4) = 2\mathrm{mod}\,(P_+; \mathrm{i}, 0, b, a + \mathrm{i})$$

where P_+ is the polygon with vertices i, 0, b, and $a + \mathrm{i}$ (see Fig. 5 (left)). If $b = a + 1$, then by (4.3), the exact value of the modulus is given by

$$\mathrm{mod}\,(R; z_1, z_2, z_3, z_4) = \frac{\pi}{\mu(k)}, \quad k = \frac{1 - 2\lambda\lambda'}{1 + 2\lambda\lambda'}, \quad \lambda = \mu^{-1}\left(\frac{\pi}{2(2a+1)}\right), \quad \lambda' = \sqrt{1 - \lambda^2}.$$

For $b = a + 1$, the proposed method is used with $n = 2^{13}$ to compute approximate values of $\mathrm{mod}\,(P_+; \mathrm{i}, 0, z_3, z_4)$ for several values of a. The relative error in the computed values is presented in Fig. 5 (right). For other values of b, let the real function $u(a, b)$ be defined for $(a, b) \in [1, 3] \times [1, 3]$ by

$$u(a, b) = 2\mathrm{mod}\,(P_+; \mathrm{i}, 0, b, a + \mathrm{i}). \tag{4.4}$$

The values of the function $u(a, b)$ are computed for several values of a, b using the above-proposed method and using the SC Toolbox. The contour lines of the values of the function u for the proposed method are presented in Fig. 6 (left). In Fig. 6 (right), we present the absolute value of the difference between the values of the function u obtained by the above method and by the SC Toolbox.

4.4 Polycircular trapezoid

In this example, we consider the trapezoid T_ϵ with the vertices $z_1 = 0$, $z_2 = 1 + \mathrm{i}\tan\pi\sigma$, $z_3 = 1 + \mathrm{i}(L + \tan\pi\beta)$, $z_4 = \mathrm{i}L$, and with a small curvature at the left side parametrized the angle $\pi\epsilon$ (see Fig. 7 (left)). This trapezoid has been considered theoretically in [3, p.

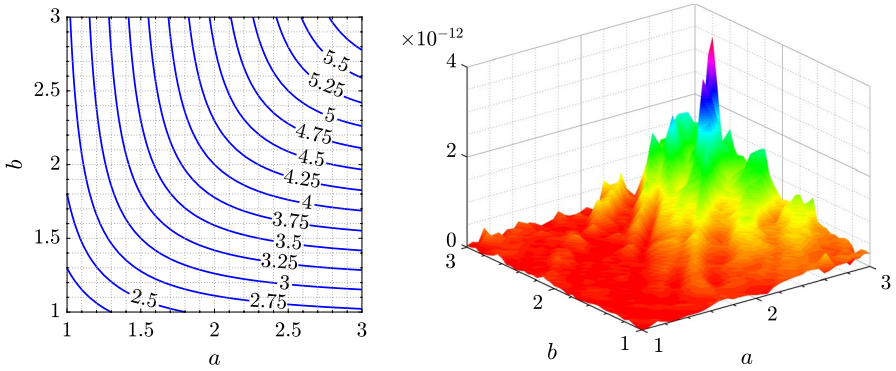

Fig. 6 The contour lines of the function $u(a, b)$ (left) the absolute value of the difference between the values of the function u obtained by the presented method and by the SC Toolbox

14] where a new formula is derived with which we are able to compare our numerical results below.

In this paper, we use the above method with $n = 2^{12}$ to compute approximate values of the modulus $\mathrm{mod}\,(T_\epsilon; z_1, z_2, z_3, z_4)$ for several values of $0.0001 \le \epsilon \le 0.25$. The values of the computed modulus is presented in Fig. 7 (right) for $L = 2$, $\sigma = \pi/8$ and $\beta = \pi/4$.

For $\epsilon = 0$, an asymptotic formula for the capacity is given by [3, Eq. (74)]

$$\mathrm{mod}\,(T_\epsilon; z_1, z_2, z_3, z_4) = \frac{2\mu(k)}{\pi}, \quad k = \sqrt{t_0} \tag{4.5}$$

where

$$\begin{aligned} t_0 =& 16e^{-\pi\hat{L}}\Big(1 - 8(1 + 4\sigma\beta)e^{-\pi\hat{L}} + 4\big(11 + 4\sigma^2 + 4\beta^2 + 128\sigma\beta + 304\sigma^2\beta^2\big)e^{-2\pi\hat{L}} \\ &+ O\Big(e^{-3\pi\hat{L}}\Big)\Big), \\ \hat{L} =& L + \frac{1}{\pi}(\Psi(0.5 + \beta) + \Psi(0.5 - \sigma) - 2\Psi(0.5)), \end{aligned}$$

and $\Psi(z) = \Gamma'(z)/\Gamma(z)$ is the digamma function. Here, t_0 is approximated by

$$t_0 \approx 16e^{-\pi\hat{L}}\Big(1 - 8(1 + 4\sigma\beta)e^{-\pi\hat{L}} + 4\big(11 + 4\sigma^2 + 4\beta^2 + 128\sigma\beta + 304\sigma^2\beta^2\big)e^{-2\pi\hat{L}}\Big).$$

Figure 8 presents the absolute values of the difference between the approximate values of the modulus obtained with our method and with the formula (4.5) for several values of $0 \le \sigma \le 0.25$ and $\epsilon = 0$, $L = 2$, $\beta = 0.25$. It follows from the definition of $\hat{L}$ that the values of $\hat{L}$ decrease as σ increases. Thus, it is expected that the

difference between the approximate values of the modulus increase as σ increases since t_0 is approximated to within $O\left(e^{-3\pi\hat{L}}\right)$.

4.5 *L*-shaped domains: polygonal boundary

Consider the simply connected domain interior to the polygon with the vertices $v_1 = -1 + 3\mathrm{i}$, $v_2 = -1 + \mathrm{i}$, $v_3 = -1 - \mathrm{i}$, $v_4 = 1 - \mathrm{i}$, $v_5 = 3 - \mathrm{i}$, $v_6 = 3 + \mathrm{i}$, $v_7 = 1 + \mathrm{i}$, and $v_8 = 1 + 3\mathrm{i}$ (see [39, p. 44]). We consider here v_2 and v_4 as vertices.

The L-shaped domain with four vertices (in counterclockwise orientation) is a quadrilateral. There are 280 possible choices of such quadrilaterals. The proposed method is used with $n = 2^{13}$ to compute the modulus for these 280 quadrilaterals and the reciprocal error based on the identity (2.2), i.e., the *reciprocal error* in Tables 2 and 3 is defined by

$$\left|1 - \mathrm{mod}\,(L;z_1,z_2,z_3,z_4)\,\mathrm{mod}\,(L;z_2,z_3,z_4,z_1)\right|. \tag{4.6}$$

The results are presented in Fig. 10 (left).

Extensive numerical tests [18] related to capacity computation show that the reciprocal error (4.6) agrees with several other error estimates. However, for the current proposed method, the reciprocal error is not significant because the method is based on mapping the domain D and the four points z_1, z_2, z_3, z_4 on its boundary to the unit disk $\mathbb{B}^2$ with four points w_1, w_2, w_3, w_4 on the unit circle. Then $\mathrm{mod}\,(\mathbb{B}^2, w_1, w_2, w_3, w_4)$ is computed using the exact formula. Note that the reciprocal error in $\mathrm{mod}\,(D, z_1, z_2, z_3, z_4)$ is the same as the reciprocal error in $\mathrm{mod}\,(\mathbb{B}^2, w_1, w_2, w_3, w_4)$. Thus, the reciprocal error in our method measures only the error in the numerical computation of the special function "μ" in the exact formula.

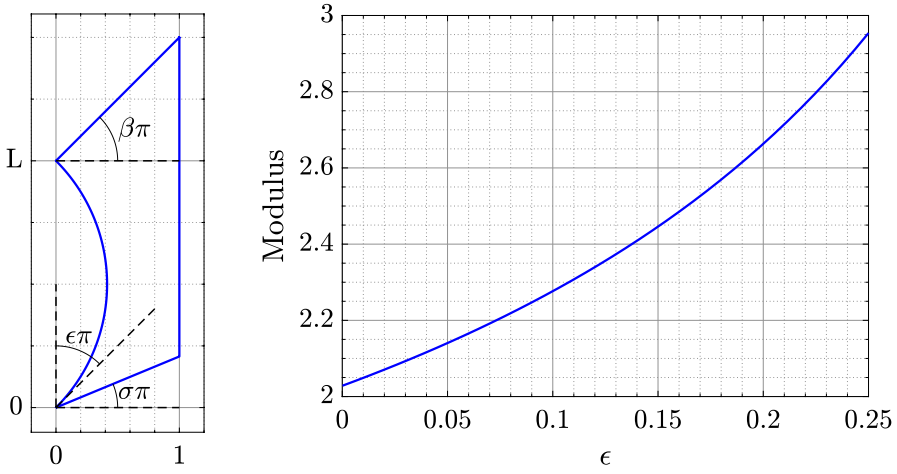

Fig. 7 The trapezoid T_ϵ (left) and the values of its modulus (right)

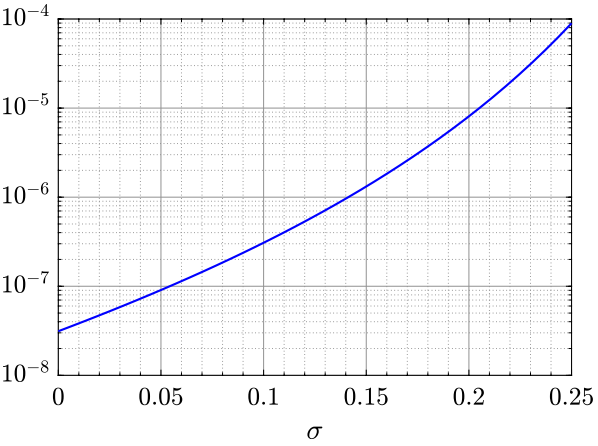

Fig. 8 The absolute values of the difference between the approximate values of the modulus obtained with our method and with the formula (4.5)

Table 2 The values of the modulus of the L-shaped quadrilateral for several choices of vertices

z_1, z_2, z_3, z_4	mod $(L; z_1, z_2, z_3, z_4)$	Exact Modulus	Relative Error	Reciprocal Error
v_1, v_3, v_5, v_6	1.73205080757599	1.73205080756888	4.11×10^{-12}	1.11×10^{-15}
v_5, v_6, v_7, v_8	1.73205080756327	1.73205080756888	3.24×10^{-12}	4.44×10^{-16}
v_1, v_3, v_5, v_7	0.99999999999876	1.00000000000000	1.24×10^{-12}	1.11×10^{-16}
v_8, v_4, v_6, v_7	0.78170096135130	0.78170096134806	4.15×10^{-12}	2.22×10^{-16}
v_8, v_1, v_3, v_6	1.70916888656242	1.70916888655749	2.88×10^{-12}	2.22×10^{-16}
v_8, v_1, v_5, v_6	2.55852314235398	2.55852314234188	4.73×10^{-12}	9.77×10^{-16}
v_8, v_2, v_4, v_6	1.56340192270204	1.56340192269611	3.79×10^{-12}	6.66×10^{-16}

Table 3 The values of the modulus of the L-shaped (circular arc) quadrilateral for several choices of vertices

z_1, z_2, z_3, z_4	mod $(L; z_1, z_2, z_3, z_4)$
v_1, v_3, v_5, v_6	1.74325313824307
v_5, v_6, v_7, v_8	1.58841772274399
v_1, v_3, v_5, v_7	1.10535075580239
v_8, v_4, v_6, v_7	0.84849597438205
v_8, v_1, v_3, v_6	1.72040886827649
v_8, v_1, v_5, v_6	2.58094977005996
v_8, v_2, v_4, v_6	1.57581541654770

For this example, the exact values of the modulus of the L-shaped quadrilateral for several choices of vertices are given in [14]. Table 2 presents these exact values as well as the approximate values obtained with the proposed method and the relative error in the approximate values. In this example, as well as in the next example, the auxiliary point α in (3.1) need to be chosen carefully to ensure the convergence of the method. In our numerical computation we choose α inside the domain

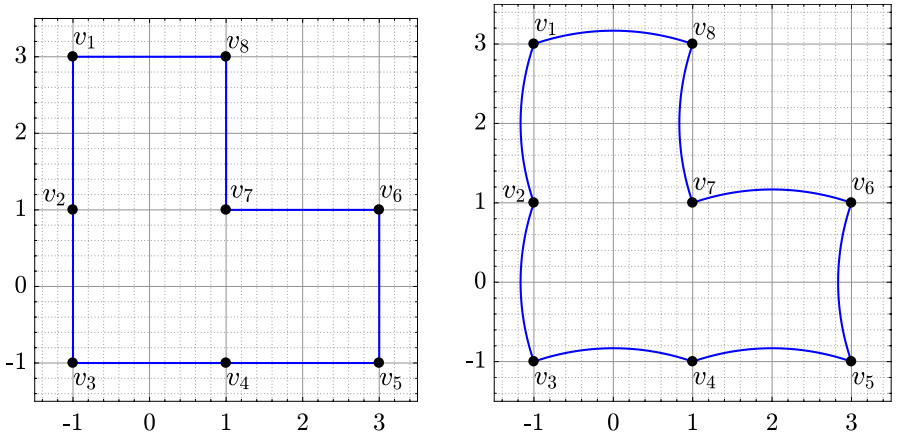

Fig. 9 Left: *L*-shaped quadrilateral. Right: The same with circular arc boundary curves

L, sufficiently far from the boundary, and close to the arithmetic mean of the vertices z_1, z_2, z_3, z_4 of the quadrilateral $(L;z_1, z_2, z_3, z_4)$.

4.6 *L*-shaped domains: polycircular boundary

Now, we consider a polycircular domain with the same vertices as in Example 4.10 (see Fig. 9 (right)). This polygon is obtained by replacing each side-segments in the polygon in Fig. 9 (left) by a circular arc such that the angle between the segment and the tangent to the circular arc is ϵ. We consider here $\epsilon = 1/3$. The proposed method is used with $n = 2^{13}$ to compute the modulus for the 280 possible choices of quadrilaterals and the reciprocal error based on the identity (2.2). The obtained results are presented in Fig. 10 (right). The values of the modulus of this *L*-shaped quadrilateral for several choices of vertices are given in Table 3.

4.7 Polycircular boundary

Consider the polygon with vertices $v_1 = -2 - 2\mathrm{i}$, $v_2 = 0.4 - 2\mathrm{i}$, $v_3 = 1.4 - 2\mathrm{i}$, $v_4 = 2 - 2\mathrm{i}$, $v_5 = 2 + 0.8\mathrm{i}$, $v_6 = -0.6 + 0.8\mathrm{i}$, and $v_7 = -2 - 0.6\mathrm{i}$ (see [44, Fig.6]). This polygon consists of 5 straight segments and 2 circular arcs with centers $0.9 - 2\mathrm{i}$ and $-2 + 0.8\mathrm{i}$, respectively (see Fig. 11).

There are 140 possible choices of four vertices z_1, z_2, z_3, z_4 to get a quadrilateral. The proposed method is used with $n = 7 \times 2^{10}$ to compute the modulus for these 140 quadrilaterals and the approximate values of the modulus for some of these choices are presented in Table 4.

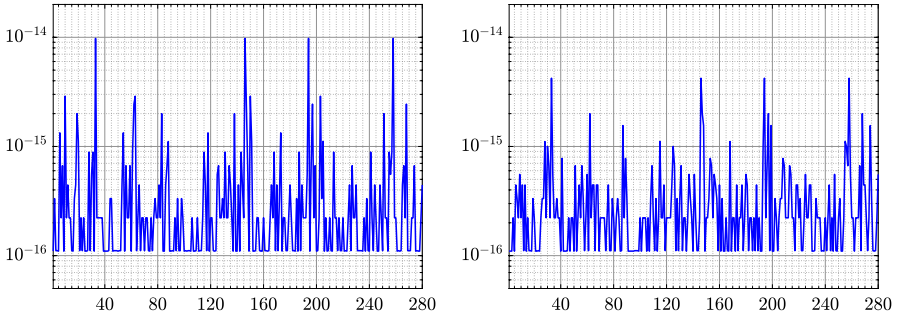

Fig. 10 Left: The reciprocal error for the *L*-shaped quadrilateral. Right: The same with circular arc boundary curves

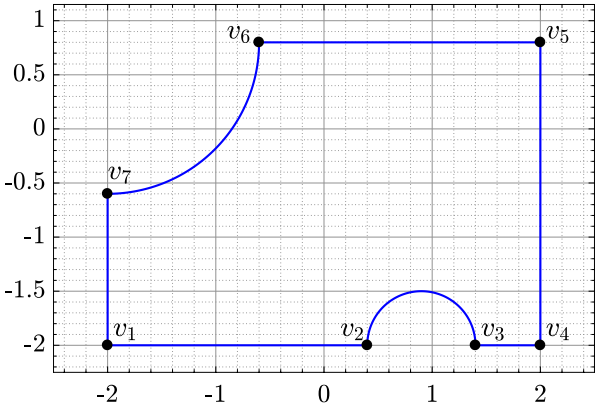

Fig. 11 The polycircular domain with 5 straight segments and 2 circular arcs defined in Section 4.7

5 Examples: exterior modulus of quadrilaterals

In this section, we consider several numerical examples to illustrate the accuracy of the proposed method for computing the exterior modulus of quadrilaterals. In the first example, the exact value of the exterior modulus is known. For the second example, we compare the above proposed method against the methods presented in [19].

5.1 Rectangle

In this example, we consider the rectangle R with the vertices $z_1 = a$, $z_2 = 0$, $z_3 = \mathrm{i}b$, $z_4 = a + \mathrm{i}b$, with $a, b > 0$. The exact value of the exterior modulus of the quadrilateral $(R; z_1, z_2, z_3, z_4)$ is given by [19, 2.3]

$$\operatorname{mod}(R; z_1, z_2, z_3, z_4) = \frac{1}{\pi}\,\mu(k), \tag{5.1}$$

where

$$k = \psi^{-1}\left(\frac{a}{b}\right), \quad \psi(k) = \frac{2(\mathcal{E}(k) - (1-k)\mathcal{K}(k))}{\mathcal{E}'(k) - k\mathcal{K}'(k)}.$$

In our numerical examples below, we assume that $a = 1$ and we choose several values of k such that $0.02787 \le k \le 0.7306$, then $0.02 < b = 1/\psi(k) < 10$. For these values of b, the proposed method with $n = 2^{13}$ is used to compute approximate values of the exterior modulus of the quadrilateral $(R;z_1, z_2, z_3, z_4)$. The relative error in the computed approximate values obtained with $n = 2^{13}$ is presented in Fig. 12 where the exact values of the exterior modulus are computed with (5.1). Further, Fig. 13 presents the relative error in the approximate values of the exterior modulus of the rectangle with $b = 2.5$ obtained by the presented method for several values of n. Similar to Fig. 3, Fig. 13 indicates that the error in the current example is also $O(n^{-4})$.

5.2 Two polygonal quadrilaterals

In this example, we compute the exterior modulus for two polygonal quadrilaterals from [19] (see Fig. 14). For the first quadrilateral, we consider the polygon P_1 with the vertices $z_1 = 1$, $z_2 = 0$, $z_3 = -19/25 + \mathrm{i}21/25$, $z_4 = 28/25 + \mathrm{i}69/50$. In the second quadrilateral, we consider the polygon P_2 with the vertices $z_1 = 1$, $z_2 = 0$, $z_3 = -3/25 + \mathrm{i}21/25$, $z_4 = 42/25 + 4\mathrm{i}$. The exact values of the exterior moduli of the quadrilaterals $(P_1;z_1, z_2, z_3, z_4)$ and $(P_2;z_1, z_2, z_3, z_4)$ are unknown. The approximate values of the exterior moduli for these two quadrilaterals are given in Table 5 obtained with the proposed method with $n = 2^{13}$. Table 5 presents also the values of the exterior modulus computed by three methods in [19], and the values computed by the explicit formula which has been recently derived in [37] for the exterior modulus of convex polygonal quadrilateral, and also the values computed by the SC toolbox in [19].

Table 4 The values of the modulus of the polycircular domain with 5 straight segments and 2 circular arcs defined in Section 4.7

z_1, z_2, z_3, z_4	mod $(L;z_1, z_2, z_3, z_4)$
v_1, v_2, v_3, v_4	2.45771442325834
v_1, v_2, v_3, v_5	1.35593720891099
v_1, v_2, v_3, v_6	1.05881208405979
v_1, v_2, v_3, v_7	0.61626814533203
v_1, v_2, v_4, v_5	1.36608045307310
v_1, v_2, v_4, v_6	1.06274475848552
v_1, v_2, v_4, v_7	0.61717041892812
v_1, v_2, v_5, v_7	1.21717866219720
v_1, v_2, v_5, v_7	0.64658016206138
v_1, v_2, v_6, v_7	0.70102635018388

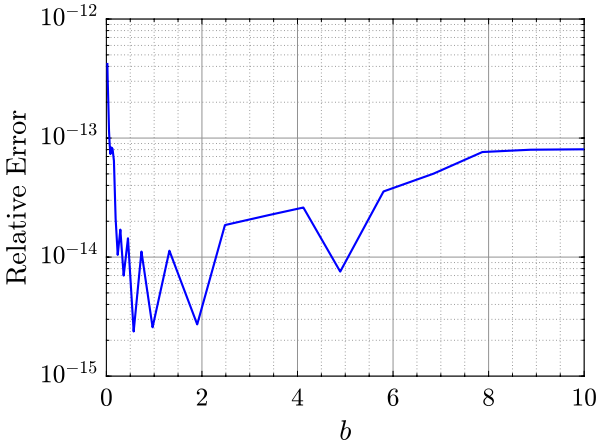

Fig. 12 The relative error in the computed approximate values of the exterior modulus of the rectangle obtained with $n = 2^{13}$ vs. b

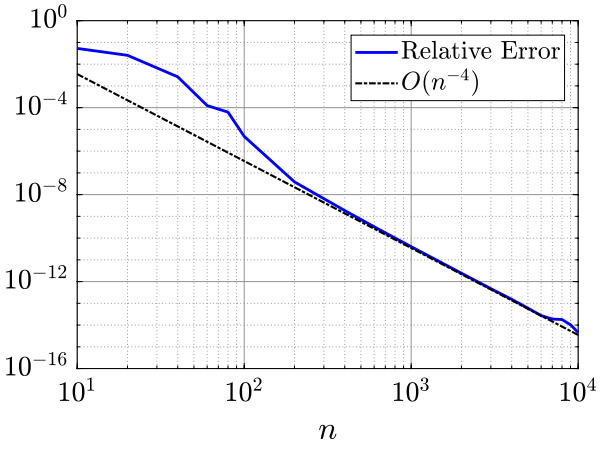

Fig. 13 The relative error in the approximate values of the exterior modulus of the rectangle with $b = 2.5$ vs. n

5.3 A polygonal quadrilateral

The (interior) modulus of the polygonal quadrilateral $(P; 0, 1, A, B)$ as well as the exterior modulus the polygonal quadrilateral $(P; 1, 0, B, A)$ for several values of A and B are computed in this example using the above-presented method with $n = 2^{13}$. The values of A and B are chosen to be the same values in [37, Table 3] where the exterior modulus has been computed in [37] using an explicit formula derived there. The values of the computed exterior modulus as well as the values computed in [37] are presented in Table 6. The absolute value of the differences between the computed values is given also in Table 6. Table 7 presents the computed values of the (interior) modulus computed by the presented method and the explicit formula given in [33, Theorem 4.11] as well as the absolute value of the differences between the computed values. Finally, it is worth mentioning that computing the explicit formulas in [33, 37] is not an easy task. However, accurate numerical methods for computing these formulas numerically are presented in [33, 37].

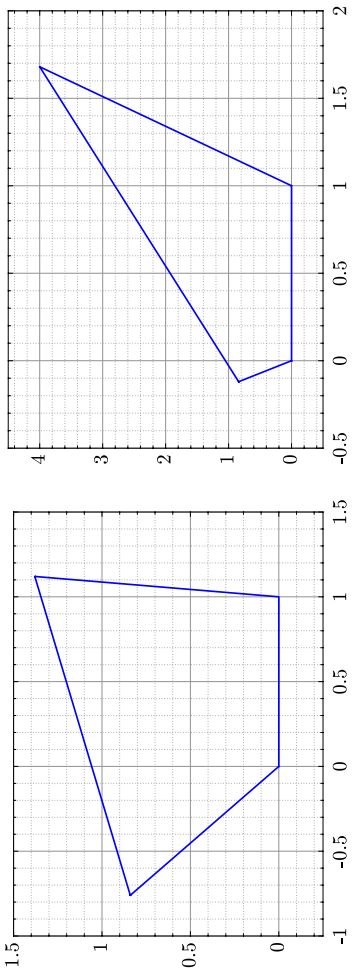

Fig. 14 The polygon P_1 (left) and the polygon P_2 (right)

Table 5 The values of the exterior modulus for the two quadrilaterals $(P_1;z_1,z_2,z_3,z_4)$ and $(P_2;z_1,z_2,z_3,z_4)$

Method	$(P_1;z_1,z_2,z_3,z_4)$	$(P_2;z_1,z_2,z_3,z_4)$
Our Method	0.992341633098101	0.959257172916209
Explicit Formula [37]	0.992341633097863	0.959257171919002
SC Toolbox [19]	0.9923416323	0.9592571721
AFEM [19]	0.9923500126	0.9593012739
hp-FEM (Interior) [19]	0.9923416332	0.9592571731
hp-FEM (Exterior) [19]	0.9923416332	0.9592572007

Table 6 The values of the exterior modulus of the quadrilaterals (P; 1, 0, B, A)

A	B	Our Method	Nasyrov et al. [37]	Agreement
7 + 5i	−1 + 2i	1.158095606012769	1.158095606321043	3.08×10^{-10}
8 + 3i	−1 + i	1.130410080967415	1.130410084465672	3.50×10^{-09}
5 + 5i	−3 + i	1.233703270045470	1.233703270301942	2.56×10^{-10}
7 + 4i	−3 + 3i	1.274708413841454	1.274708414007269	1.66×10^{-10}
5 + 5i	−1 + 2i	1.140576491968641	1.140576491710462	2.58×10^{-10}
7 + 5i	i	1.015468483039331	1.015468479689712	3.35×10^{-09}
7 + 3i	1 + 2i	1.135151674880489	1.135151674872885	7.60×10^{-12}
4 + 5i	−2 + i	1.157883901208362	1.157883901548636	3.40×10^{-10}
1 + i	i	0.999999999999998	0.999999999999995	3.00×10^{-15}

Table 7 The values of the (interior) modulus of the polygonal quadrilateral (P; 0, 1, A, B)

A	B	Our Method	Nasser et al. [33]	Agreement
7 + 5i	−1 + 2i	1.173365891585431	1.173365891585535	1.04×10^{-13}
8 + 3i	−1 + i	0.718534280250316	0.718534280248976	1.34×10^{-12}
5 + 5i	−3 + i	1.001711782988431	1.001711782988453	2.11×10^{-14}
7 + 4i	−3 + 3i	1.178216101417496	1.178216101417495	6.66×10^{-16}
5 + 5i	−1 + 2i	1.273824771478209	1.273824771478195	1.44×10^{-14}
7 + 5i	i	0.922232203043405	0.922232203042563	8.42×10^{-13}
7 + 3i	1 + 2i	1.685745608775185	1.685745608775512	3.27×10^{-13}
4 + 5i	−2 + i	1.024798809022298	1.024798809022340	4.22×10^{-14}
1 + i	i	1.000000000000000	1.000000000000000	8.88×10^{-16}

Table 8 The vertices v_k and the preimages w_k for the gear domain with 6 vertices

k	v_k	w_k
1	$e^{i\pi/5}$	0.97953567010215 + 0.20127064117138i
2	$0.75e^{i\pi/5}$	0.92181215666441 + 0.38763687624595i
3	$0.75e^{3i\pi/5}$	−0.60224821653432 + 0.79830889114505i
4	$1.25e^{3i\pi/5}$	−0.82674608972861 + 0.56257524218406i
5	$1.25e^{3i\pi/2}$	−0.33447524422818 − 0.94240453680917i
6	$e^{3i\pi/2}$	−0.20794689838982 − 0.97814011647108i

6 Conformal mapping onto gear domains

6.1 Gear domains

A gear domain D is a special case of the polycircular domains described above. It is a simply connected domain starlike with respect to the origin and bordered by arcs of circles centered at the origin and segments of lines passing through the origin [7–9, 40] . Here, we assume that D is bounded.

Gear domains and the computation of the conformal mapping from the unit disk onto a gear domain with one tooth have been studied intensively by Brown and Porter in [7–9] . The method is based on using the Schwarzian derivative of the Riemann mapping. The method can be used to compute also the modulus of the gear domain. Several results related to the modulus and geometry of gear domains were presented in [9].

In this section, the boundary integral method presented in Section 3 is used to compute the conformal mapping $w = \Phi(z)$ for the gear domain D onto the unit disk $\mathbb{B}^2$ normalized by (3.14) as well as its inverse $z = \Phi^{-1}(w)$ from $\mathbb{B}^2$ onto D. Assume that D has m vertices v_k, $k = 1, 2, \ldots, m$. Then the method can be used to compute also the preimages w_k, $k = 1, 2, \ldots, m$, of these vertices. The method is used also to compute the (internal) modulus of gear domains as well as the external modulus. The presented results illustrate the effectivity and the accuracy of the presented method. Our results confirm the theoretical results in [9]. In particular, in Section 6.3, we shall present a numerical validation of a conjecture presented in [9].

6.2 A gear domain with 6 vertices

As our first example, we consider a gear domain with 6 vertices. This example has been considered in [40, Fig. 4(b)] (although the vertices of this domain are not given explicitly in [40], we approximate these vertices from Fig. 4(b) in [40]). The vertices are given in Table 8.

The method presented in Section 3.4 is used with $n = 3 \times 2^{11}$ to compute the conformal mapping from the gear domain D onto the unit disk and its inverse. Figure 15 (left) shows the images of several circles $|w| = r$, for $r = 0.3, 0.45, 0.6, 0.75, 0.9$, in the unit disk under the inverse conformal mapping $z = \Phi^{-1}(w)$. The image of the circle $|z| = r$ or part of the circle for $r = 0.19, 0.58, 0.88, 1.13$, in the domain D under the conformal mapping $w = \Phi(z)$ is shown in Fig. 15 (right). The square markers on

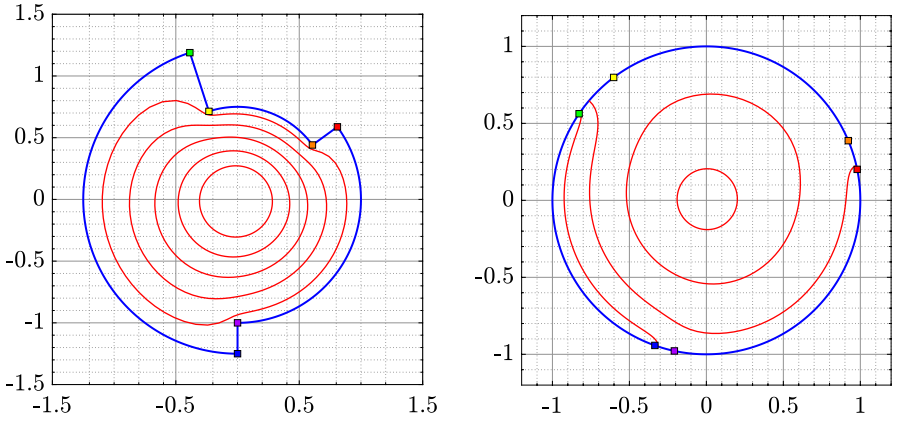

Fig. 15 The gear domain with 6 vertices (left) and the unit disk (right)

the unit circle are the preimages of the vertices of the gear domain. The approximate values of the preimages are presented in Table 8.

6.3 One-tooth gear domain

Numerical conformal mappings onto one-tooth gear domains have been considered in [7–9]. Without loss of generality, a one-tooth gear domain is a polycircular domain with the vertices $v_1 = e^{-i\theta}$, $v_2 = \beta e^{-i\theta}$, $v_3 = \beta e^{i\theta}$, and $v_4 = e^{i\theta}$ where $0 < \theta < \pi$ is the gear angle and $\beta > 1$ is the gear ratio [8]. The method presented in Section 3.4 is used with $n = 2^{13}$ to compute the conformal mapping from the gear domain D onto the unit disk and its inverse for $\beta = 1.5$ and $\theta = \pi/6$. Figure 16 (left) shows the images of several circles $|w| = r$, for $r = 0.09, 0.19, \ldots, 0.99$, under the inverse conformal mapping $z = \Phi^{-1}(w)$. The image of the circle $|z| = r$ or part of the circle for $r = 0.09, 0.19, \ldots, 1.49$, under the conformal mapping $w = \Phi(z)$ is shown in Fig. 16 (right). The square markers on the unit circle indicate the preimages of the vertices of the gear domain.

For fixed values of β and for $0 < \theta < \pi$, the modulus of the quadrilateral $(D; e^{-i\theta}, \beta e^{-i\theta}, \beta e^{i\theta}, e^{i\theta})$ has been computed with the proposed method with $n = 2^{13}$ and the results are presented in Fig. 17. As proved in [9, Proposition 3.3 (ii)], the computed values of the modulus approachzero as $\theta \to 0$ or $\theta \to \pi$. Further, the results presented in Fig. 17 validate numerically the conjecture in [9, p. 90]. That is, there are exactly two gears corresponding to two differentvalues of θ with the same modulus except for one value of $\theta \in (0, \pi)$ where the modulus has its maximum value. These maxima are marked with squares in Fig. 17.

The location of the maximum value depends on the value of β. These locations, i.e., the values of θ corresponding to the maximum values of the modulus of the quadrilateral $(D; e^{-i\theta}, \beta e^{-i\theta}, \beta e^{i\theta}, e^{i\theta})$ are presented in Fig. 18 as a function of β. These values of θ are in the interval $(\pi/2, \pi)$, move toward $\pi/2$ as $\beta \to 1^+$ and move toward π as $\beta \to \infty$. Moreover, for $0 < \theta < \pi$, the value of the modulus is a monotone decreasing function of β, see Fig. 19.

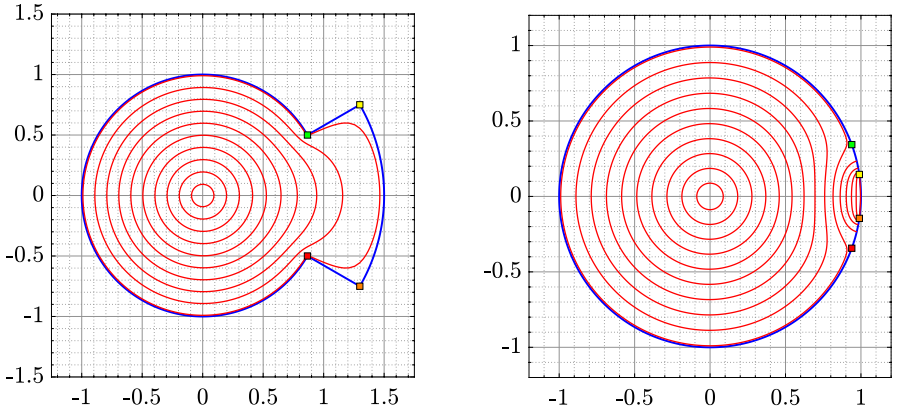

Fig. 16 The gear domain with one-tooth for $\theta = \pi/6$ and $\beta = 1.5$ (left) and the unit disk (right)

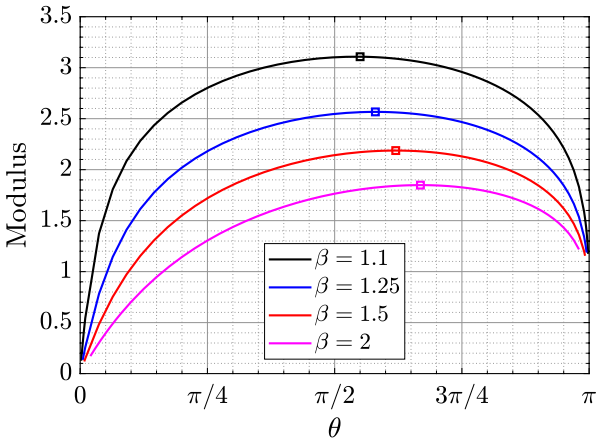

Fig. 17 The modulus of the quadrilateral $\left(D;e^{-i\theta},\beta e^{-i\theta},\beta e^{i\theta},e^{i\theta}\right)$

In conclusion, these observations confirm the result presented in [9, Proposition 3.3 (i)] that the modulus approaches ∞ as $\beta \to 1^+$ and approaches 0 as $\beta \to \infty$. Finally, Fig. 20 presents the contour lines of the modulus of the quadrilateral $\left(D;e^{-i\theta},\beta e^{-i\theta},\beta e^{i\theta},e^{i\theta}\right)$ as a function of θ and β for $\pi/20 \le \theta \le 19\pi/20$ and $1.05 \le \beta \le 4$.

6.4 A multitooth gear domain

We consider a multitooth gear domain with 12 vertices as in Table 9. The method presented in Section 3.4 is used with $n = 3 \times 2^{12}$ to compute the conformal mapping from the gear domain D onto the unit disk and its inverse. Figure 21 (left) shows the images of several circles $|w| = r$, for $r = 0.09, 0.19, \ldots, 0.99$, under the inverse conformal mapping $z = \Phi^{-1}(w)$. The image of the circle $|z| = r$ or part of the circle for $r = 0.09, 0.19, \ldots, 1.99$, under the conformal mapping $w = \Phi(z)$ is shown in Fig. 21 (right).

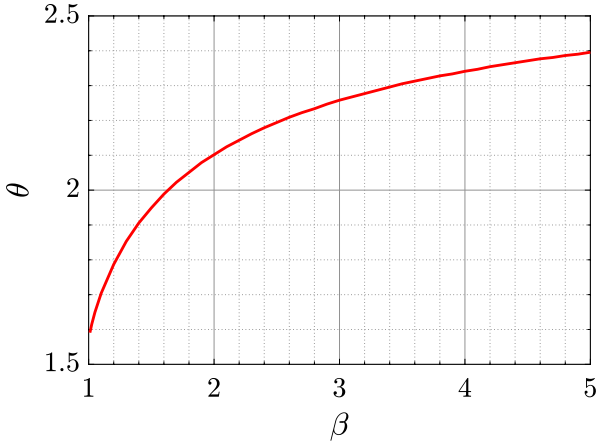

Fig. 18 The values of θ corresponding to the maximum value of the modulus of the quadrilateral $\left(D;e^{-i\theta},\beta e^{-i\theta},\beta e^{i\theta},e^{i\theta}\right)$ as a function of β

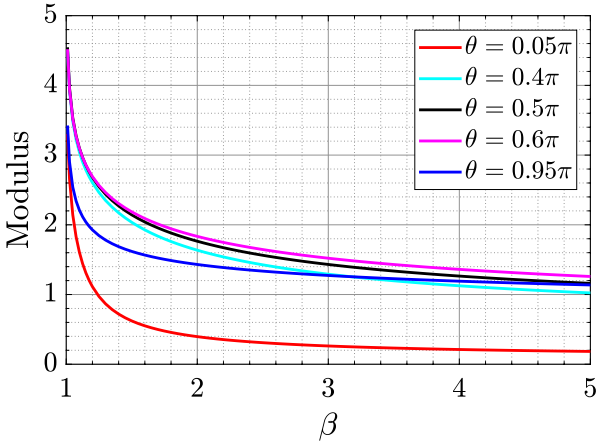

Fig. 19 The values of the modulus of the quadrilateral $\left(D;e^{-i\theta},\beta e^{-i\theta},\beta e^{i\theta},e^{i\theta}\right)$

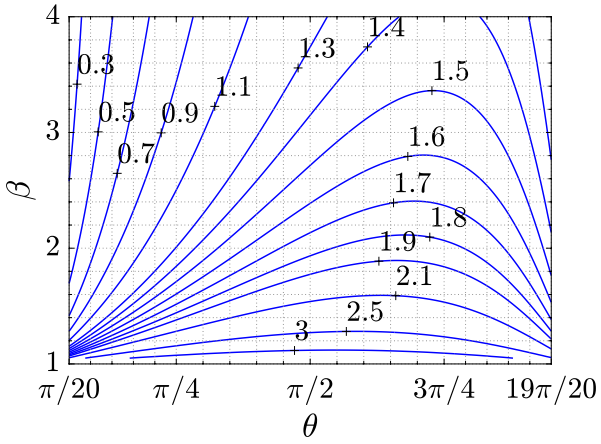

Fig. 20 The contour lines of the values of the modulus of the quadrilateral $\left(D;e^{-i\theta},\beta e^{-i\theta},\beta e^{i\theta},e^{i\theta}\right)$ as a function of θ and β

Table 9 The vertices v_k and the preimages w_k for the multitooth gear domain with 12 vertices

k	v_k	w_k
1	$e^{i\pi/6}$	0.86701428817497 + 0.49828327696246i
2	$e^{i\pi/2}$	−0.28316473230969 + 0.95907128743174i
3	$2e^{i\pi/2}$	−0.56900711726358 + 0.82233259725210i
4	$2e^{3i\pi/4}$	−0.65069062054555 + 0.75934295040781i
5	$1.5e^{3i\pi/4}$	−0.71186505065025 + 0.70231627466742i
6	$1.5e^{i\pi}$	−0.95549393111898 + 0.29501075843909i
7	$1.25e^{i\pi}$	−0.97908358634907 + 0.20345842558580i
8	$1.25e^{3i\pi/2}$	−0.62508676492722 − 0.78055527434822i
9	$0.75e^{3i\pi/2}$	−0.32775376595675 − 0.94476318138524i
10	$0.75e^{11i\pi/6}$	0.97086850902193 − 0.23961289236922i
11	$1.75e^{11i\pi/6}$	0.98506920087238 + 0.17215884959145i
12	$1.75e^{i\pi/6}$	0.95294901093885 + 0.30313063611365i

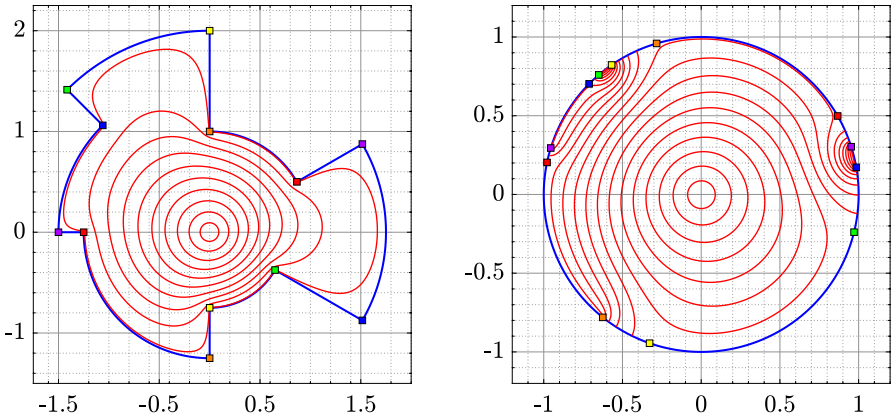

Fig. 21 The multitooth gear domain (left) and the unit disk (right)

6.5 Complement of an annular rectangle

Consider the polycircular domain whose boundary consists of the straight segment from $e^{-i\theta}$ to $\beta^2 e^{-i\theta}$, the circular arc from $\beta^2 e^{-i\theta}$ to $\beta^2 e^{i\theta}$, the straight segment from $\beta^2 e^{i\theta}$ to $e^{i\theta}$, and the circular arc from $e^{i\theta}$ to $e^{-i\theta}$ where $\theta \in (0, \pi)$ and $\beta > 1$ (see domain G in Fig. 22 for $\theta = \pi/4$ and $\beta = 1.5$). This domain G is called an *annular rectangle* [8]. Consider also the gear domain D with the vertices $e^{-i\theta}$, $\beta e^{-i\theta}$, $\beta e^{i\theta}$, and $e^{i\theta}$ (see domain D in Fig. 22). Then, it follows from [8, Theorem 6.1] that the exteriormodulus of the quadrilateral $\left(G; e^{-i\theta}, \beta^2 e^{-i\theta}, \beta^2 e^{i\theta}, e^{i\theta}\right)$ is half of mod $\left(D; e^{-i\theta}, \beta e^{-i\theta}, \beta e^{i\theta}, e^{i\theta}\right)$.

In this example, we use our proposed method with $n = 2^{13}$ to compute the exterior modulus of the quadrilateral $\left(G; e^{-i\theta}, \beta^2 e^{-i\theta}, \beta^2 e^{i\theta}, e^{i\theta}\right)$ as well as mod $\left(D; e^{-i\theta}, \beta e^{-i\theta}, \beta e^{i\theta}, e^{i\theta}\right)$ for several values of θ. The absolute value of the difference

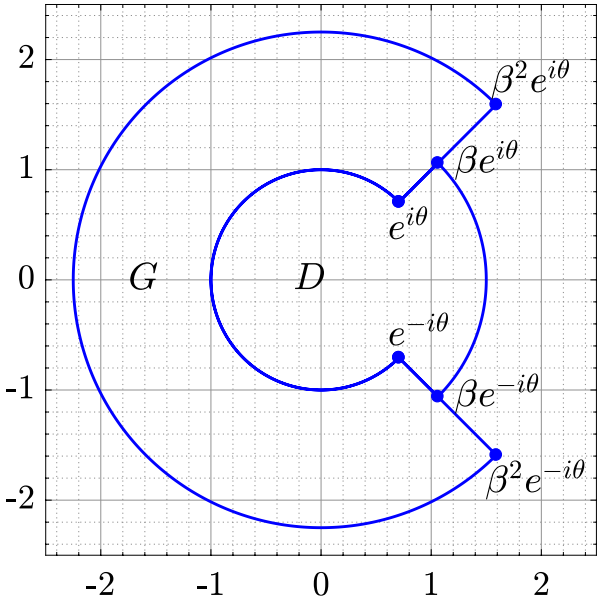

Fig. 22 The annular rectangle domain G and the gear domain D

Table 10 The exterior modulus of the quadrilateral $\left(G;e^{-i\theta},\beta^2e^{-i\theta},\beta^2e^{i\theta},e^{i\theta}\right)$ and mod $\left(D;e^{-i\theta},\beta e^{-i\theta},\beta e^{i\theta},e^{i\theta}\right)$

θ	Exterior modulus	0.5 mod $\left(D;e^{-i\theta},\beta e^{-i\theta},\beta e^{i\theta},e^{i\theta}\right)$	Error
0.1π	0.51830606688359	0.51830606688379	1.96×10^{-13}
0.2π	0.77581840983574	0.77581840983561	1.30×10^{-13}
0.3π	0.92576131108263	0.92576131108211	5.21×10^{-13}
0.4π	1.01795618251692	1.01795618251687	4.91×10^{-14}
0.5π	1.07133752300218	1.07133752300216	1.40×10^{-14}
0.6π	1.09298754180547	1.09298754180560	1.27×10^{-13}
0.7π	1.08332598419075	1.08332598419105	2.95×10^{-13}
0.8π	1.03535729272694	1.03535729272677	1.68×10^{-13}
0.9π	0.92271712140416	0.92271712140442	2.59×10^{-13}

between the computed exterior modulus and 0.5 mod $\left(D;e^{-i\theta},\beta e^{-i\theta},\beta e^{i\theta},e^{i\theta}\right)$ is considered as the error in the computed values. The obtained results are presented in Table 10.

Acknowledgements We would like to thank the referees for their careful work.

Funding Open Access funding provided by University of Turku (UTU) including Turku University Central Hospital. O. Rainio's research was funded by the University of Turku Graduate School UTUGS. A. Rasila and T. Wallace were funded by National Natural Science Foundation of China (No. 11971124) and

Natural Science Foundation of Guangdong Province (No. 2021A1515010326). H. Yu and X. Zhang were supported by the Natural Science Foundation of Zhejiang Province (LY22A010004).

Data availability All the data used in the research for this article was created with MATLAB codes available in GitHub at https://github.com/mmsnasser.

Declarations

Conflict of interest The authors declare no competing interests.

References

1. Ablowitz, M.J., Fokas, A.S.: Complex Variables: Introduction and Applications. Cambridge Texts in Applied Mathematics, 2nd edn., p. xii+647. Cambridge University Press, Cambridge (2003)
2. Ahlfors, L.V.: Conformal Invariants: Topics in Geometric Function Theory. McGraw-Hill Series in Higher Mathematics. McGraw-Hill Book Co., New York-Düsseldorf-Johannesburg (1973)
3. Anselmo, T., da Cunha, B., Nelson, R., Crowdy, D.G.: Schwarz-Christoffel accessory parameter for quadrilaterals via isomonodromy. J. Phys. A: Math. Theor. **53**, 355201 (2020)
4. Bauer, U., Lauf, W.: Conformal mapping onto a doubly connected circular arc polygonal domain. Comput. Methods Funct. Theory **19**(1), 77–96 (2019)
5. Bjørstad, P., Grosse, E.: Conformal mapping of circular arc polygons. SIAM J. Sci. Stat. Comput. **8**, 19–32 (1987)
6. Bottazzini, U., Gray, J.: Hidden Harmony – Geometric Fantasies. The Rise of Complex Function Theory. Sources and Studies in the History of Mathematics and Physical Sciences, pp. xviii+848. Springer, New York (2013). ISBN: 978-1-4614-5724-4; 978-1-4614-5725-1
7. Brown, P.R.: Conformal mapping of a gear domain with one tooth. Quaest. Math. **33**, 277–289 (2010)
8. Brown, P.R., Porter, R.M.: Numerical conformal mapping to one-tooth gear-shaped domains and applications. Comput. Methods Funct. Theory **16**(2), 319–345 (2016)
9. Brown, P.R., Porter, R.M.: Gears, pregears and related domains. Complex Var. Elliptic Equ. **61**, 89–103 (2016)
10. Crowdy, D.: Solving Problems in Multiply Connected Domains. CBMS-NSF Regional Conference Series in Applied Mathematics, 97. Society for Industrial and Applied Mathematics (SIAM), Philadelphia, PA, (2020)
11. Driscoll, T.A.: Schwarz–Christoffel Toolbox for MATLAB. https://tobydriscoll.net/project/sc-toolbox/. Accessed 11 May 2021
12. Driscoll, T.A., Trefethen, L.N.: Schwarz-Christoffel Mapping. Cambridge Monographs on Applied and Computational Mathematics, 8, p. xvi+132. Cambridge University Press, Cambridge (2002)
13. Dubinin, V.N.: Condenser Capacities and Symmetrization in Geometric Function Theory, Birkhäuser, (2014)
14. Gaier, D.: Ermittlung des konformen Moduls von Vierecken mit Differenzenmethoden. Numer. Math. **19**, 179–194 (1972)

15. Gehring, F.W., Martin, G.J., Palka, B.P.: An Introduction to the Theory of Higher-Dimensional Quasiconformal Mappings. Mathematical Surveys and Monographs, 216. American Mathematical Society, Providence, RI, pp. ix+430 (2017)
16. Greengard, L., Gimbutas, Z.: FMMLIB2D: A MATLAB toolbox for fast multipole method in two dimensions, version 1.2. (2019) www.cims.nyu.edu/cmcl/fmm2dlib/fmm2dlib.html. Accessed 6 Nov 2020
17. Hakula, H., Quach, T., Rasila, A.: The conjugate function method and conformal mappings in multiply connected domains. SIAM J. Sci. Comput. **41**(3), A1753–A1776 (2019)
18. Hakula, H., Rasila, A., Vuorinen, M.: On moduli of rings and quadrilaterals: algorithms and experiments. SIAM J. Sci. Comput. **33**(1), 279–302 (2011)
19. Hakula, H., Rasila, A., Vuorinen, M.: Computation of exterior moduli of quadrilaterals. Electron. Trans. Numer. Anal. **40**, 1–16 (2013) ISSN 1068-9613
20. Hariri, P., Klén, R., Vuorinen, M.: Conformally Invariant Metrics and Quasiconformal Mappings. Springer Monographs in Mathematics. Springer, Berlin (2020)
21. Henrici, P.: Applied and Computational Complex Analysis, vol. 3. John Wiley & Sons, New York (1986)
22. Howell, L.H.: Numerical conformal mapping of circular arc polygons. J. Comput. Appl. Math. **46**, 7–28 (1993)
23. Kress, R.: A Nyström method for boundary integral equations in domains with corners. Numer. Math. **58**(2), 145–161 (1990)
24. Kress, R.: Boundary integral equations in time-harmonic acoustic scattering. Math. Comput. Modelling **15**, 229–243 (1991)
25. Kress, R.: Linear Integral Equations. Applied Mathematical Sciences, 82, 3rd edn., p. xvi+412. Springer, New York (2014)
26. Kythe, P.K.: Handbook of Conformal Mappings and Applications, p. xxxv+906. CRC Press, Boca Raton (2019)
27. Liesen, J., Séte, O., Nasser, M.M.S.: Fast and accurate computation of the logarithmic capacity of compact sets. Comput. Methods Funct. Theory **17**, 689–713 (2017)
28. Nasser, M.M.S.: Numerical conformal mapping via a boundary integral equation with the generalized Neumann kernel. SIAM J. Sci. Comput. **31**, 1695–1715 (2009)
29. Nasser, M.M.S.: Fast solution of boundary integral equations with the generalized Neumann kernel. Electron. Trans. Numer. Anal. **44**, 189–229 (2015)
30. Nasser, M.M.S.: Fast computation of the circular map. Comput. Methods Funct. Theory **15**, 187–223 (2015)
31. Nasser, M.M.S.: PlgCirMap: A MATLAB toolbox for computing the conformal mapping from polygonal multiply connected domains onto circular domains. SoftwareX **11**, 100464 (2020). arXiv 2019, arXiv:1911.01787
32. Nasser, M.M.S., Murid, A.H.M., Zamzamir, Z.: A boundary integral method for the Riemann-Hilbert problem in domains with corners. Complex Var. Elliptic Equ. **53**, 989–1008 (2008)
33. Nasser, M.M.S., Rainio, O., Vuorinen, M.: Condenser capacity and hyperbolic perimeter. Comput. Math. Appl. **105**, 54–74 (2022)
34. Nasser, M.M.S., Vuorinen, M.: Numerical computation of the capacity of generalized condensers. J. Comput. Appl. Math. **377**, 112865 (2020)
35. Nasser, M.M.S., Vuorinen, M.: Conformal invariants in simply connected domains. Comput. Methods Funct. Theory **20**, 747–775 (2020)
36. Nasser, M.M.S., Vuorinen, M.: Computation of conformal invariants. Appl. Math. Comput. **389**, 125617 (2021)
37. Nasyrov, S., Sugawa, T., Vuorinen, M.: Moduli of quadrilaterals and quasiconformal reflection. (2021) arXiv:2111.08304
38. Papamichael, N.: Gaier's contributions to numerical conformal mapping. Comput. Methods Funct. Theory **3**, 1–53 (2003)
39. Papamichael, N., Stylianopoulos, N.: Numerical Conformal Mapping: Domain Decomposition and the Mapping of Quadrilaterals. pp. xii+229. World Scientific Publishing Co. Pte. Ltd., Hackensack, NJ (2010)
40. Pearce, K.: A constructive method for numerically computing conformal mappings for gearlike domains. SIAM J. Sci. Stat. Comput. **12**, 231–246 (1991)

41. Pólya, G., Szegö, G.: Isoperimetric Inequalities in Mathematical Physics. Annals of Mathematics Studies, no. 27, pp. xvi+279. Princeton University Press, Princeton, N. J (1951)
42. Porter, R.M.: History and Recent Developments in Techniques for Numerical Conformal Mapping. Quasiconformal mappings and their applications, pp. 207–238. Narosa, New Delhi (2007)
43. Porter, R.M.: On the art of calculating accessory parameters of conformal mappings of circular arc polygons–general considerations and special situations. Teichmüller theory and moduli problem, 549–576, Ramanujan Math. Soc. Lect. Notes Ser., 10, Ramanujan Math. Soc., Mysore (2010)
44. Trefethen, L.N.: Numerical Conformal Mapping with Rational Functions. Comput. Methods Funct. Theory **20**, 369–387 (2020)
45. Wegmann, R.: Methods for numerical conformal mapping. In: R. Kühnau (ed.), Handbook of Complex Analysis: Geometric Function Theory, Vol. 2, pp. 351–477. Elsevier B. V., (2005)
46. Wegmann, R., Murid, A.H.M., Nasser, M.M.S.: The Riemann-Hilbert problem and the generalized Neumann kernel. J. Comput. Appl. Math. **182**, 388–415 (2005)